Nuclear Instruments and Methods in Physics Research A295 (1990) 102–108
North-Holland

A glass spherical Cherenkov counter based on total internal reflection

C. Biino, A. Ceccucci, R. Cester, F. Marchetto, E. Menichetti *, A. Migliori,
R. Mussa, S. Palestini, N. Pastrone, L. Pesando and G. Rinaudo
Dipartimento di Fisica Sperimentale dell'Università di Torino and INFN, Sezione di Torino, 10125 Torino, Italy

G. Borreani and V. Carassiti
Istituto di Fisica dell'Università di Ferrara and INFN, Sezione di Ferrara, 44100 Ferrara, Italy

Received 26 February 1990 and in revised form 14 May 1990

We built and tested a Cherenkov counter for particle identification, with spherical shape ($R = 600$ mm), made of glass. The threshold at $\beta = 0.92$ is set by the mechanism of total internal reflection of the Cherenkov light.

1. Introduction

Cherenkov-radiation emission has been extensively used in charged-particle identification. Many applications approached the problem by considering the natural threshold linked to the radiator refractive index n by the well known relation $\beta_{\text{thres}} = 1/n$. A charged particle crossing a radiator at a speed greater than $\beta_{\text{thres}}c$ emits Cherenkov photons; in a threshold Cherenkov counter, these photons are collected through an optical system by a photoelectric transducer, and the outcoming signal is used to discriminate particles with speed above threshold from those below threshold. The choice of the refraction index is determined by the kinematics of the processes under study, and of course has limitations related to the existence of a medium having the desired optical properties.

To increase the spectrum of technically achievable thresholds, a substantially different way of operating a Cherenkov counter was devised based on the threshold for total internal reflection (t.i.r.) of the emitted light in a refractive medium [1]. Consider a Cherenkov radiator in the form of a plate with parallel plane surfaces, transparent to light, immersed in a medium having a refractive index smaller than the index n of the plate, for instance glass in air. The plate is orthogonal to the particle direction. For $\beta > 1/n$, Cherenkov photons will be produced and they will impinge on the glass–air interface with an incidence angle equal to the Cherenkov angle $\theta_c = \arccos(1/\beta n)$.

For small Cherenkov angles, the light is partially reflected and partially transmitted, and escapes the plate after a few of these processes; however, for sufficiently high β values the light is trapped inside the plate and can be collected at the end of it. This occurs when the incidence angle θ_i is greater than the critical angle θ_{crit} for total internal reflection: $\theta_i > \theta_{\text{crit}} = \arcsin(n_0/n)$ where n_0 is the air refractive index. The threshold is then simply given by

$$\beta_{\text{t.i.r.}} = 1/\sqrt{n^2 - n_0^2}. \quad (1)$$

For instance, plexiglas ($n = 1.49$) in air would give a t.i.r. threshold at $\beta = 0.906$, while that for a conventional Cherenkov counter would require a radiator with an index of refraction equal to 1.1, not easy to produce.

Within the planar geometry described, total-reflection-threshold counters have been frequently used for beam particle identification.

In this paper we report on the construction and performance of a spherically shaped counter based on total internal reflection and designed to be used as part of a pointing geometry detector.

The counter was developed as a prototype to investigate the possibility of an upgrade of the detector of Experiment 760 at Fermilab [2] devoted to the study of the process $p\bar{p} \to \phi\phi \to K^+K^-K^+K^-$ at $E_{\text{c.m.}}$ around 3.0 GeV.

Two major requirements must be satisfied in order to isolate the above process from the vast background of annihilations into pions:

a) multipion final-state rejection at trigger level;
b) minimal amount of material in the counter assembly, to keep multiple scattering small and preserve a good performance of the charged-particle tracking system

* Now at Istituto di Fisica dell'Università di Udine, 33100 Udine, Italy.

0168-9002/90/$03.50

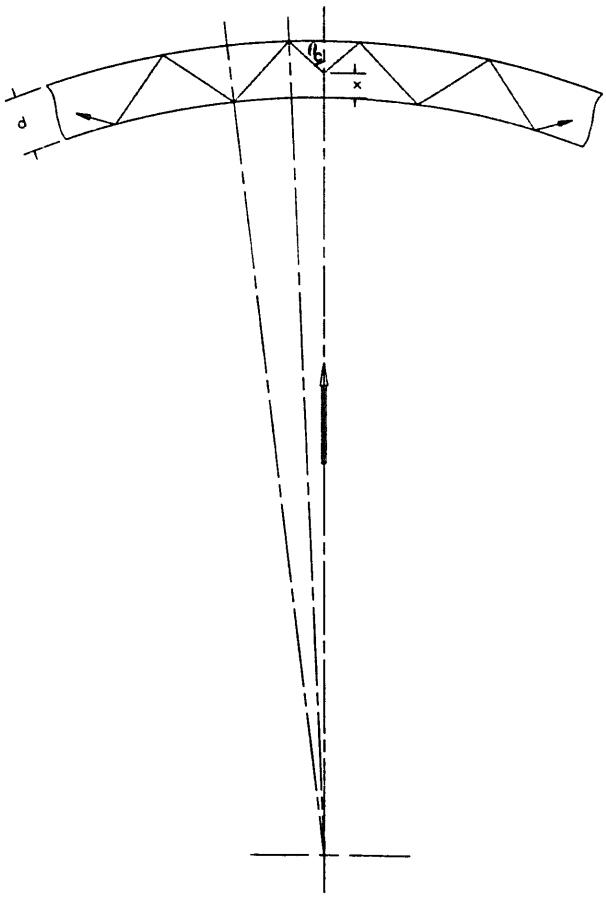

Fig. 1. Sketch of the total-internal-reflection mechanism.

that is crucial for off-line reconstruction and kinematical fit [3]; this feature is also important for the planned simultaneous detection of the $\gamma\gamma$ final state.

2. Principle of operation of a spherical counter

Fig. 1 illustrates the path followed by Cherenkov photons in a central geometry. Notice that photons produced by a particle coming from the center of curvature have incidence angles on the outer (inner) surface of the radiator smaller (greater) than the Cherenkov angle; moreover, both incidence angles are a function of the position of the point of emission along the particle path. For a shell of thickness d, inner radius R, index n, immersed in a medium with index n_0, the threshold velocity ($\beta_{\text{t.i.r.}}(x)$), for emission occurring at depth x within the shell, is given by the relation

$$\beta_{\text{t.i.r.}}(x) = \left[n^2 - n_0^2 \left(\frac{R+d}{R+x} \right)^2 \right]^{-1/2} . \qquad (2)$$

For increasing particle velocity, the condition for total internal reflection is first achieved by photons radiated just before the exit from the plate ($x = d$), and full trapping will be achieved only when the velocity will be sufficiently high to have the photons emitted just after the entrance ($x = 0$) also totally internally reflected. This results in a smooth threshold with onset at a value of β given by eq. (1), and a width proportional to the ratio d/R. Above threshold, the light yield is expected to rise according to the $\sin^2\theta_c$ behaviour of the Cherenkov cross section.

3. The prototype

We built a prototype conceptually equal to one of 24 elements that will compose the whole counter. The radiator element, sketched in fig. 2a, is a segment of a

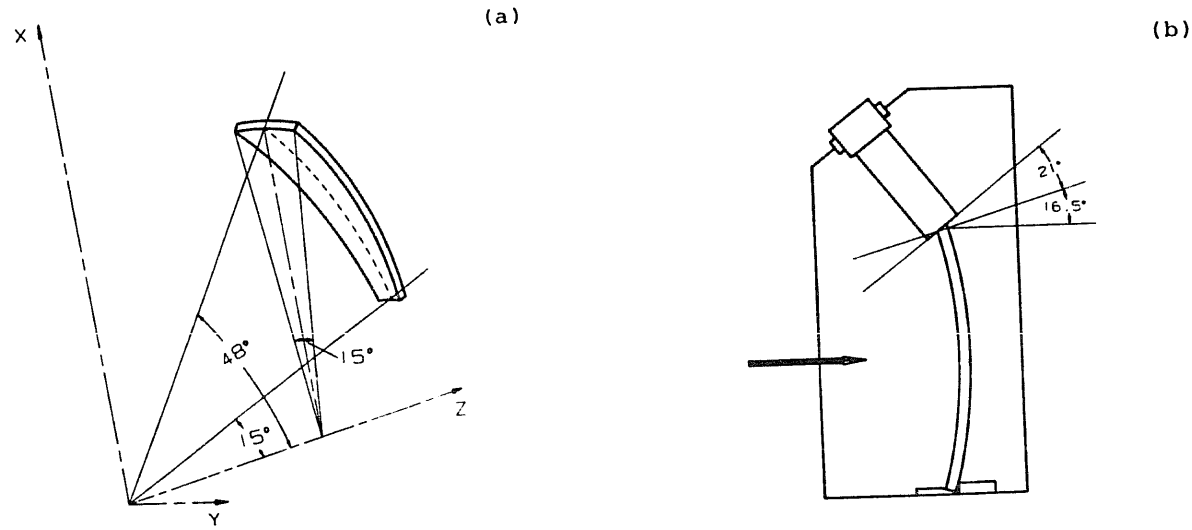

Fig. 2. (a) Sketch of a single element of the counter, and (b) schematic cross section of the prototype.

Table 1
FK3 characteristics; the refractive index is for $\lambda = 400$ nm and the internal transmittance is measured for 25 mm and $\lambda = 400$ nm.

Refractive index	Internal transmittance	Density [g cm^{-3}]	T.i.r. momentum threshold [GeV/c]		
			π	K	P
1.4763	0.960	2.25	0.333	1.178	2.239

spherical shell of FK3-type glass [4] cut to correspond to an acceptance of $2\pi/24$ in the azimuthal angle, and 15° to 48° in the polar angle, and is supported inside a light-tight box with 1 mm thick brass walls; two XP2262 photomultipliers (2 in. diameter) collected the light trapped in the glass. The photomultipliers are kept in contact with the glass end surface by means of optical grease. Three radiators of different thickness were tried, all having the smaller radius of curvature equal to 600 mm. The inside surface of the box was covered with black felt. Fig. 2b shows a schematic cross section of the box; notice the 21° tilt of the photomultiplier windows with respect to the radial direction. This is motivated by space constraints on the photomultipliers position in the real experiment.

The FK3 glass main characteristics are listed in table 1 together with the nominal momentum threshold from eq. (1) for π/K/p. This glass is well suited to separate kaons from pions up to 1.2 GeV/c.

In the next section we give some details on the technique used to construct the glass radiator.

4. Glass construction

In a geometry pointing to the interaction region, the curvature precision and the smoothness of the glass surfaces are of primary importance: any deviation might cause the light to escape, worsening the threshold definition. Moreover, the FK3 glass is rather expensive and a method had to be devised to avoid machining a thick block of glass down to the desired spherical shape.

Starting from a commercially available plate with dimensions ($l = 450$, $w = 160$, $d = 20$) mm^3, the mechanical process to obtain the spherical shape consisted of two steps: 1) bend the glass to the correct curvature; 2) cut and polish to produce the proper dimensions and smoothness of the surfaces.

The bending procedure here described was developed at CERN and is a modified version of the method used to form spherical mirrors [5]. The glass plate to be bent was layed in horizontal position inside a concave spherical ($R = 620$ mm) cast iron mould having a diameter ($\varnothing = 490$ mm) larger than the plate. The whole assembly was heated to 560°C and the FK3 glass, made plastic by the heat, bent under the action of gravity to assume the curvature of the mould. The mould and the glass were covered with a thin film of boron nitrate to facilitate disassembling.

Finally, the glass was cut and polished by using standard techniques and tooling. The two spherical surfaces were concentric within a tolerance that corresponded to less than 0.1 mm difference in thickness over the whole counter.

All six surfaces (two spherical and four plane) of the glass were polished to reach optical quality. The two side surfaces (i.e. those corresponding to $\varphi = \pm 7.5°$ in fig. 2a) were coated with 1000 Å aluminum, resulting in an approximate 90% reflectivity at 400 nm. This feature was not strictly necessary for this prototype, since total internal reflection would have worked equally well as reflection on aluminum. However, it will be important for the final counter because it will allow a simple assembly design with small cracks and no cross talk between adjacent glasses.

5. Test setup and results

During a preliminary test performed at the T10 test beam of the CERN PS, we used a glass 19.5 mm thick, with inner radius of curvature equal to 600 mm, and proved that the principle of the total-internal-reflection counter works also in a spherical geometry. Subsequently we built two other elements with the same inner radius, 8 and 12 mm thick, and tested all of them at the Brookhaven National Laboratory.

The goals of these tests were:

1) to measure the distribution of the photomultipliers signal as a function of particle velocity from below t.i.r. threshold to $\beta > 0.99$, to assess efficiency and rejection power when using the counter as veto;
2) to optimize the choice of thickness of the radiator glass;
3) to study the variation of response with the position of impact of the particle on the counter.

The test was performed using the B2 beam at the BNL-AGS. The negative-beam composition was mainly pions with approximately 1% antiproton contamination. Since the kaons component was negligible we used antiprotons (pions) to study the counter behaviour below (above) t.i.r. threshold.

The trigger was defined by three scintillation counters, S_1, S_2 (dimensions $h = w = 100$ mm) and S_3 (dimensions $h = w = 10$ mm), placed along the beam line. S_1 was placed 46 cm upstream of the glass counter, while S_2 and S_3 were 28 and 100 cm downstream, respectively. Two multiwire proportional chambers (2 x, y planes each, with 1 mm pitch), installed 48 cm upstream and 32 cm downstream of the counter, were part of the system to determine the beam-particle direc-

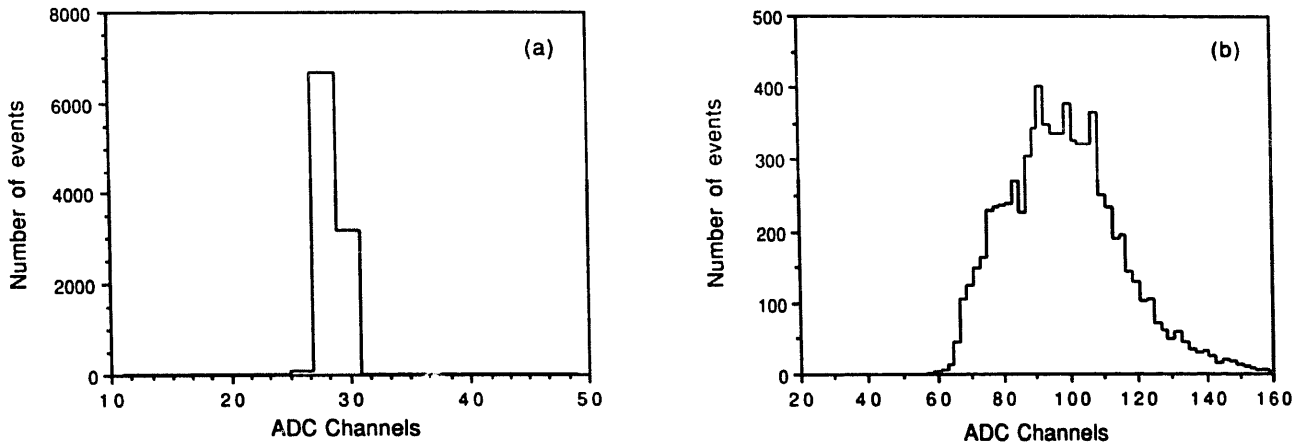

Fig. 3. (a) Typical pulse-height distribution for a pedestal run, and (b) for photomultiplier noise (1 photoelectron).

tion. A time-of-flight measurement to identify antiprotons was performed by using the scintillation counter S_2 together with another counter S_0 placed 18.8 m upstream.

The signals from the glass photomultipliers were amplified by a factor 10 and digitized with a LeCroy 4300 FERA. The gain of the whole chain was systematically monitored measuring the signal corresponding to the noise of the photomultipliers. Figs. 3a and 3b show a typical ADC channel distribution for pedestal and noise (1 photoelectron) respectively. From the relative position of the two peaks one finds the calibration constant needed to count photoelectrons (1 pe corresponded to about 65 ADC channels). Gain instabilities, mainly due to temperature variations, were approximately equal to 5%.

Data were taken with beam momenta ranging from 1.0 to 3.0 GeV/c.

The off-line trigger selection was designed to isolate a clean sample of single well-collimated beam tracks. This was achieved by imposing two requirements; a) one cluster of hits per chamber plane to reject multiple track triggers; b) angle between the track and the beam axis passing through the center of curvature of the counter less than 1°. This cut discarded tracks not compatible with the requirement of coming from an interaction region of 1 cm^3 as expected in Experiment 760.

The time-of-flight measurement of the events passing the above cuts allowed the antiproton identification. A typical distribution of S_2-S_0 time is shown in fig. 4 for a beam momentum of 1.75 GeV/c. The time resolution (rms) is approximately equal to 400 ps, well suited to guarantee a $\pi/\bar{p}$ separation up to 3.0 GeV/c, where antiprotons are well above t.i.r. threshold. For the rest of this paper, pion and antiproton identification is based on the time-of-flight measurement.

The signals from the two photomultipliers were normalized to represent number of photoelectrons and finally summed. Figs. 5a and 5b show the distributions of the number of photoelectrons from π's and $\bar{p}$'s at 1.75 GeV/c, from the 12 mm thick counter and the beam centered at $\theta = 31.5°$ and $\varphi = 0°$ (the counter central position). The superimposed curves are the results of a fit of the data to a Poisson distribution, giving $\langle N_{pe} \rangle = 15.4 \pm 0.8$ for π's and $\langle N_{pe} \rangle = 0.3 \pm 0.05$ for $\bar{p}$'s. The errors include the uncertainty on the horizontal scale.

As expected, the two distributions show a striking difference: the antiprotons ($\beta = 0.881$) are below threshold and therefore most of the Cherenkov light escapes the glass, while π's have $\beta = 0.997$ (well above threshold), light is trapped in the glass and a significant part of it can reach the photomultipliers. Considering in more detail the antiproton signal distribution, we notice that approximately 26% of the events shows a signal which is not compatible with them being pedestals. Various phenomena could contribute to the excess of

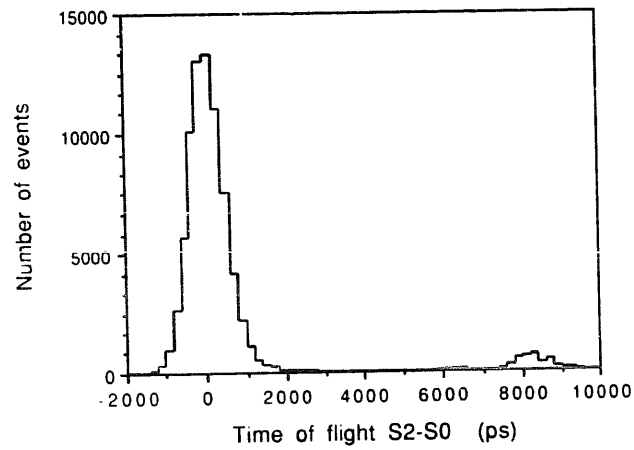

Fig. 4. S_2-S_0 time-of-flight distribution at 1.75 GeV/c beam momentum; the two peaks corresponding to π's and $\bar{p}$'s (on the right) are well separated. The time-scale origin has been shifted to coincide with the pion peak.

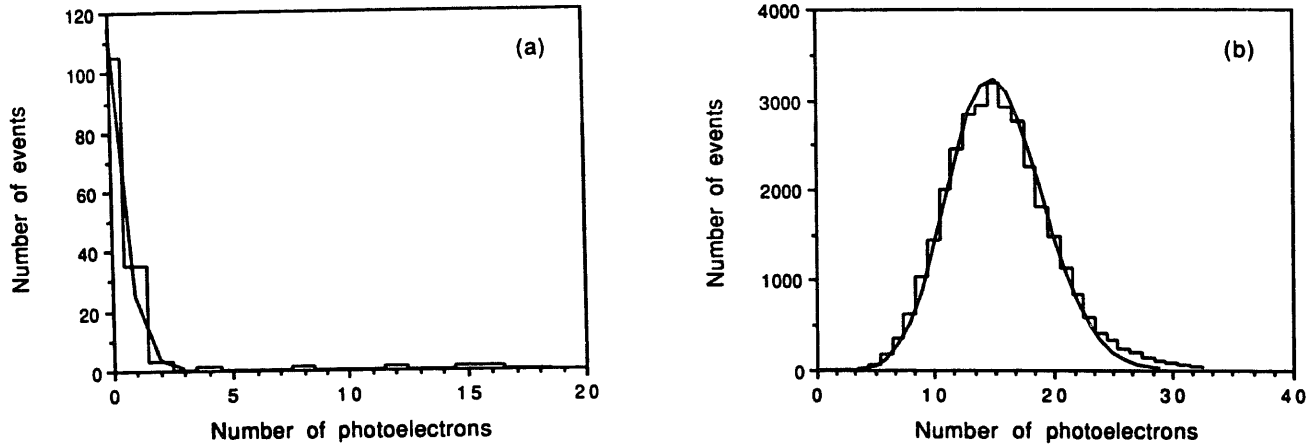

Fig. 5. Distribution of the sum of the number of photoelectrons seen by the two photomultipliers: (a) antiprotons at 1.75 GeV/c (below threshold), and (b) pions at 1.75 GeV/c (above threshold), with superimposed Poisson fits.

light: 1) δ-rays generated by antiprotons; 2) scintillation activity of the glass. An estimation of the amount of Cherenkov light emitted by δ-rays and collected by the photomultipliers gives a result compatible with the measured signal associated to $\bar{p}$ below t.i.r. threshold.

The behaviour of $\langle N_{pe} \rangle$ as a function of β is shown in fig. 6. The β threshold is evidently not sharp, an effect already discussed in section 2.

There are other factors that were not mentioned and may influence the threshold, for instance the dependency of the Cherenkov angle on the photon frequency. To try to understand the detailed shape of the threshold, we used a full Monte Carlo simulation, that incorporated the glass and beam geometry, as well as various physical effects: chromatic dispersion and absorption in the FK3 glass, features of metal reflection from glass onto aluminum, quantum efficiency of the photomultiplier with its dependency on the wavelength. Since

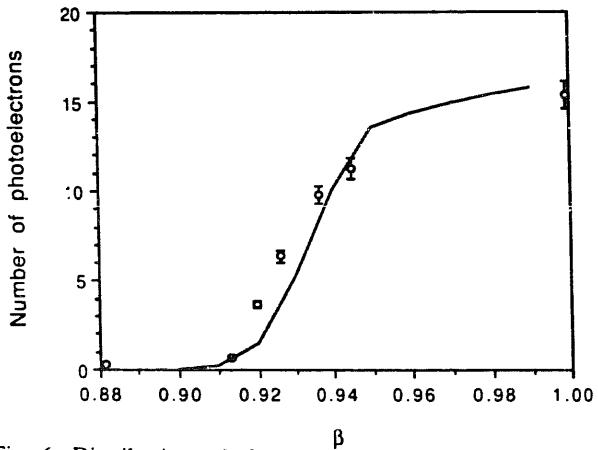

Fig. 6. Distribution of the number of photoelectrons as a function of β of the particle for experimental points and Monte Carlo results (line). The data point at $\beta = 0997$ refers to 1.75 GeV/c pions, all remaining experimental points are from the antiproton data.

reflection depends on the state of polarization, the Cherenkov photon polarization was followed through the various internal dielectric and metal reflections. Phase and amplitudes were calculated by use of complex Fresnel formulae; for the complex refractive index of aluminum we used the data of Hass and Waylonis [6].

The results of the calculation are shown by the continuous line in fig. 6. Due to the large number of reflections involved (27, on the average, in this case), the uncertainty on the absolute normalization is estimated to be approximately equal to ±15%. The experimental point collected at $\beta = 0.997$ is in good agreement with the calculation.

One can see that the experimental points at $\beta =$ 0.920, 0.927, and 0.935 exceed the Monte Carlo prediction by 1–2 photoelectrons. The discrepancy cannot be attributed to miscalibration of the beam momentum: systematic shifts greater than 25 MeV/c are ruled out upon examination of the time-of-flight measurements. Nor could we invoke for an explanation the smearing of the Cherenkov angle due to multiple scattering, which has a minor effect, and to the coherence length of the particle electric field in glass [7], calculated to be negligible.

The behaviour of the average number of photoelectrons as a function of β for the glasses with thickness 8 and 19.5 mm has a shape similar to the 12 mm thick glass. The light collection near $\beta = 1$ is equal to 8.5, 15.4, and 30 pe for the three glasses. There is a 30% difference on the number of photoelectrons per mm of path in the glass, which goes from 1.1 for 8 mm, to 1.3 for 12 mm, and 1.5 for 19.5 mm. The effect can be explained considering the number of internal reflections, which is higher for thinner counter, and assuming 1% loss at each internal reflection.

All the tests described above were done with the particle beam impinging on the glass at its central

Table 2
Response for different impact points; the uncertainties in the average number of photoelectrons are equal to ±5%.

θ	φ	$N_{pe}(\beta=1)$	$N_{pe}(\beta=0.881)$
18.5	0.0	14.7	0.5
31.5	0.0	17.9	0.6
31.5	0.0	15.4 [a]	0.3 [a]
31.5	5.5	17.6 [a]	0.8 [a]
44.5	0.0	21.6	0.9

[a] Counter in upright position: we observed an approximate 15% systematic difference when we rotated the counter by 90° about the beam direction (same impact point). This effect may be due to stray magnetic field.

position, i.e. in a configuration that will correspond to particles with $\theta = 31.5°$ and $\varphi = 0°$ during the real experiment. In principle we expect a different response when changing the impact point, this being related to the different path length and different number of reflections undergone by the light before reaching the photomultiplier.

To assess the extent of this variation, we dedicated a series of runs to measure the response of the 12 mm thick glass for various impact points of the particles. These were produced by rotating and translating the counter in a fashion appropriate to obtain the desired point on the beam axis while preserving a normal incidence of the beam on the glass.

Data were taken at 1.75 GeV/c where π's are fully relativistic ($\beta = 0.997$) and $\bar{p}$'s are below threshold for total internal reflection. Table 2, column 3, shows the average number of photoelectrons detected on π's. As expected, the signal is stronger at large θ angle, where the particle traverses the glass closer to the photomultipliers. Column 4 gives the average number of photoelectrons for antiprotons. To use the counter as an antiproton tagger, one would impose a threshold on the pulse height from the photomultiplier: only particles with pulses below threshold would be retained. The performance will be characterized by two parameters: the efficiency ϵ in tagging antiprotons, and inefficiency R_π in rejecting pions (punch-through). An example of this is illustrated in fig. 7, where $1-\epsilon$ and R_π are shown as a function of the cut on N_{pe}, for the spectra shown in Figs. 5a and 5b. One can see that this prototype can achieve rejections better than 10^{-3} with efficiency approximately equal to 97%. Similar results were obtained for all impact points. These numbers match the requirements of our experiment.

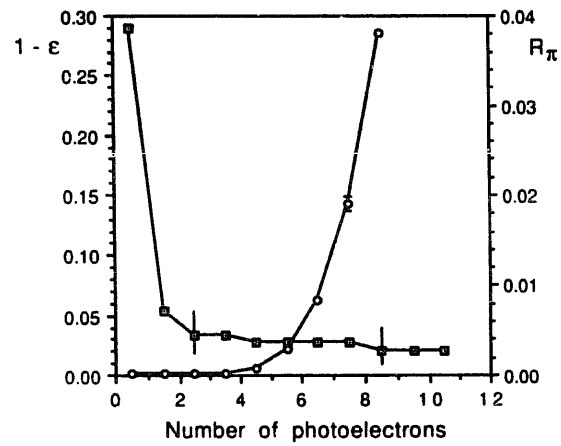

Fig. 7. Efficiency (squares) and rejection (circles) as a function of the cut on the number of photoelectrons. Some statistical error bars are shown.

6. Conclusions

We built and tested a prototype threshold Cherenkov counter based on total internal reflection and with spherical shape.

We find that, operating with a FK3 glass of thickness 12 mm and smaller radius of curvature equal to 600 mm in a veto configuration, we can obtain a rejection of particles above threshold better than 10^{-3}, while the efficiency for retaining particles below threshold is approximately equal to 97%.

The loss of transparency due to background radiation in the experimental area has been monitored. By exposing the glass to an integrated radiation of 200 rad, the reduction of the internal transmittance has been measured to be $< 1\%$ [8].

These results make feasible an upgrade of Fermilab Experiment 760 to study charmonium decays to $2K^+\,2K^-$.

Acknowledgements

We acknowledge the technical contribution of the following people: A. Braem, D. Carminati, G. Gendre, C. Nichols at CERN, A. Pecchioli at the SILO Firenze, S. Bigoni, G. Bonora at the University of Ferrara, G. Dughera and G. Giraudo at INFN, Torino. Our colleagues of the E760 collaboration: M. Savrié at the University of Ferrara and T. Armstrong at Penn State University are acknowledged for their help in performing the tests and setting up the beam line; M. Mandelkern at the University of California at Irvine is acknowledged for the radiation damage measurement.

References

[1] V. Fitch and R. Motley, Phys. Rev. 101 (1956) 496.
[2] V. Bharadwaj et al., Fermilab proposal no. 760 (March 1985).

[3] C. Baglin et al., Phys. Lett. B231 (1989) 557.
[4] Schott Glasswerke, Mainz, FRG.
[5] P. Baillon et al., Nucl. Instr. and Meth. A276 (1989) 492.
[6] G. Hass and J.E. Waylonis, J. Opt. Soc. Am. 51 (1961) 719.
[7] K.G. Dedrick, Phys. Rev. 87 (1952) 891.
[8] M. Mandelkern, private communication; the doses corresponding to a 1% reduction of light transmission as a function of the wavelength have been measured to be: 320 rad at $\lambda = 380$ nm, 365 rad at $\lambda = 400$ nm, 470 rad at $\lambda = 430$ nm, 570 rad at $\lambda = 460$ nm, 470 rad at $\lambda = 486$ nm, 480 rad at $\lambda = 520$ nm, 640 rad at $\lambda = 650$ nm.